Spectroscopy, polarization and nonadiabatic dynamics of electronically excited Ba(Ar)$_n$ clusters: Theory and experiment

A. I. Krylov and R. B. Gerber
Department of Physical Chemistry and The Fritz Haber Research Center, The Hebrew University of Jerusalem, Jerusalem 91904, Israel and Department of Chemistry, University of California, Irvine, California 92717

M. A. Gaveau, J. M. Mestdagh, B. Schilling and J. P. Visticot
CEA/DRECAM/Service de Photons Atomes et Molecules, C.E.N. Saclay, F-91191 Gif-sur-Yvette Cedex, France

(Received 13 September 1995; accepted 17 November 1995)

Molecular Dynamics simulations using a surface-hopping method for transitions between different electronic states are employed to study the dynamics following photoexcitation of the Ba(Ar)$_{125}$ cluster. The results are used to interpret spectroscopic experiments on large, size-distributed Ba(Ar)$_n$ clusters. The dynamics of the coupled electronic-nuclear motions in the cluster involves transitions between three potential energy surfaces, corresponding to the nearly-degenerate p-states of the excited Ba atom. Ejection of excited Ba atoms, adsorbed on the surface of the cluster, can take place. The focus in comparing theory and experiment is on the emission spectrum from the excited clusters, on the polarization of this radiation, and on the polarization of light emitted by excited Ba atoms ejected from the cluster. Based on the good agreement found between theory and experiment, a comprehensive picture of the excited state dynamics is given. It is found that upon excitation, energy is rapidly redistributed in the cluster and no direct ejection of Ba occurs. Electronic relaxation to the lowest P-state occurs, and the latter dominates the cluster emission spectrum and polarization. The electronic state relaxation is mostly complete within $t \lesssim 10$ ps. Ejection of Ba atoms occurs as a rare and delayed event when a dynamical fluctuation creates a ''hot spot'' at the Ba site, with a non-adiabatic excitation to the highest electronic level. The results show the feasibility of near-quantitative understanding of non-adiabatic processes in large clusters. © *1996 American Institute of Physics.* [S0021-9606(96)03108-7]

I. INTRODUCTION

The quantitative description of non-adiabatic processes in solids and liquids, or at surfaces, is among the major challenges in the theory of dynamics in condensed phases. Among the rich variety of such processes, a relatively simple example is that of an electronically excited atom immersed in a dense medium, or located at a surface. Of prime interest in these systems is the relaxation of the excited electronic state to the ground state, and radiationless transitions between different excited states in the course of the dynamics. To simulate such processes, a Molecular Dynamics method which includes non-adiabatic transitions is obviously required. For small systems, having a few atoms only, rigorous quantum mechanical calculations of the dynamics are feasible, and one can on this basis also test approximate theories. Extended or large systems are as yet outside the range of accurate quantum calculations. Therefore, it is essential to test approximate theories for such systems against experiments, and to assess their accuracy and range of validity on this basis. Another approach that is often attempted is to evaluate approximate dynamical methods for condensed phases by tests against exact calculations for small systems. Useful as the latter approach may be, it must be kept in mind that it is bound to be limited and inconclusive, since the physical factors causing possible breakdown of the method in condensed phases may be quite different than in small systems.

Work on approximation methods for non-adiabatic transitions in condensed phases has been vigorously pursued in recent years. Several very useful and promising approaches have been developed, and we mention here just a few of these. The semiclassical ''surface hopping'' method developed by Tully and by others[1–3] is based on treating nuclear motions classically, and the electronic degrees of freedom quantum-mechanically. Criteria based on the time-dependence of the electronic wavefunctions are used in an algorithm that decides whether ''hopping'' of the nuclear degrees of freedom from one potential surface to another takes place at a given point in time. The recent version of the method introduces an algorithm that minimizes the number of repeated ''hopping'' events in the potential surfaces, which seems to yield significant improvement for certain types of systems.[2] The ''surface hopping'' technique has certainly been among the most extensively used methods for nonadiabatic processes in condensed phases. The method of Rossky and co-workers[4] has several elements in common with Tully's approach, but includes in the treatment a ''quantum potential'' representing the effect of the electrons upon the nuclei at the non-adiabatic transition events. A similar method has been developed independently by Coker.[5] The

method of Meyer and Miller[6] applies a classical description to both electronic and nuclear degrees of freedom, with the advantage of a unified, elegant treatment of the entire system. Developed originally for gas-phase systems, the method can readily be extended to large, condensed-phase systems. Finally, we mention very recent work by Jungwirth and Gerber,[7] who introduced a method that treats both the electronic and the nuclear degrees of freedom quantum mechanically. While not numerically exact, there is evidence that the method provides simulations of good accuracy for short time-scales at least, and is feasible for systems much larger than hitherto treated in a full quantum-mechanical framework.[7] However, the largest non-adiabatic system simulated by this approach so far is $Ba(Ar)_{20}$, still much smaller than the systems studied here.

In the present article, we present a combined experimental and theoretical study on the photoinduced dynamics of large $Ba(Ar)_n$ clusters. A major objective is to understand in detail the dynamical mechanisms of the processes involved, and in particular to determine the nature and role of non-adiabatic processes. In the theoretical simulations here, Tully's ''surface hopping'' method is used, and the comparison with experiments provides a test for the validity of the approach. Extensive experimental study on these systems in recent years by the Saclay group, have already resulted in important insights into the processes involved.[8–15] In view of this, the large $Ba(Ar)_n$ clusters appear a very attractive model for exploring the dynamics of excited atoms adsorbed on a chemically inert surface.

The structure of the paper is as follows. Sec. II presents the theoretical method used, and the modeling of the system. Sec. III outlines the experiments carried out. Sec. IV analyzes and discusses the main theoretical and experimental results obtained, seeking to present a comprehensive view of the dynamics in this system. Brief concluding remarks are given in Sec. V.

II. THEORETICAL MODEL AND METHOD

A. Simulations of $Ba(Ar)_{125}$ in the electronic ground state

The simulations described here were carried out for $Ba(Ar)_{125}$. The experiments in the present study, to which comparisons will be made, are for a distribution of $Ba(Ar)_n$ clusters, characterized by a mean size of $n=300$, and a full-width at half-maximum of 300. It is our assumption here that for the phenomena investigated, the results are already cluster-size independent for $n \approx 125$ and beyond, in which case our model can be expected to yield properties similar to those of the experimental ensemble. It should be kept in mind, however, that in principle our model corresponds most closely to the smaller-size clusters in the experimental ensemble.

The Molecular Dynamics simulations of the cluster in its electronic ground state are necessary for generating a set of initial conditions, configurations and momenta of the atoms, for the photoexcitation dynamics. Simulations of $Ba(Ar)_n$ in the ground state were already previously reported,[15] and we only briefly discuss here the calculations carried out in the present study. The simulations are for thermally equilibrated $Ba(Ar)_{125}$. The dynamical history of the formation of the cluster, by trapping of Ba atoms in argon clusters,[8] is thus not relevant to the description of the system. The calculations were carried out for two cluster temperatures, $T=35$ K and $T=70$ K. The cluster was followed to equilibration in long MD runs (~ 40 ps), and standard MD criteria were used to test that equilibrium at the desired temperature was attained.[16] The potential function was assumed to be a sum of pairwise Ar-Ar and Ba(S)-Ar interactions. The Ar-Ar pair potential was taken from Aziz and Slaman,[17] the Ba(S)-Ar from Visticot *et al.*[15] At the temperatures studied, the geometry of the system corresponds to a Ba atom adsorbed on the surface of an approximately spherical $(Ar)_{125}$ cluster.

B. Excited-state interactions

The interactions in the manifold of the three lowest excited singlet surfaces involve a non-spherical P-state Ba atom. We used the familiar Diatomics in Molecules (DIM) model[18] to describe the interactions between this atom, including its unpaired p-orbital, and the Ar atoms. The total interaction potential between all the atoms in the cluster is written as:

$$V = U + \sum_{i>j} u(r_{ij}), \tag{1}$$

where $u(r)$ is the Ar-Ar pair potential, r_{ij} is the distance between the i and the j Ar atoms, and U represents the interaction between Ba(P) and the Ar atoms. U is approximated as a sum of pair interactions between the Ba(P) and each Ar atom:

$$U = \sum_{i=1}^{Na} U_i . \tag{2}$$

Further, U_i is expanded in Legendre polynomials, with only two terms contributing in the case of P-atom due to symmetry:[19]

$$U_i(r_i, \gamma_i) = V_0(r_i) + V_2(r_i) P_2(\cos\ \gamma_i), \tag{3}$$

where r_i is the barium distance to the argon atom, and γ_i is an electronic coordinate representing the angle between the Ba-Ar distance vector $\mathbf{r}_i$, and the orientation of the unpaired p-orbital of the Ba. The interaction U, based on electrostatic and empirical considerations, is obviously not a potential in the Born–Oppenheimer sense, since it explicitly contains an electronic degree of freedom, the orbital orientation angle. For a diatomic Ba-Ar system, the functions $V_0(r), V_2(r)$ of Eq. (3) can readily be obtained from the Σ and Π adiabatic potential energy curves:[19,20]

$$V_0(r) = \frac{1}{3}\,[W_\Sigma(r) + 2W_\Pi(r)], \tag{4}$$

$$V_2(r) = \frac{5}{3}\,[W_\Sigma(r) - W_\Pi(r)]. \tag{5}$$

The adiabatic potentials $W_\Sigma(r), W_\Pi(r)$, hence the interaction $U_i(r_i,\gamma_i)$ of Eq. (3), were taken from the work of Visticot *et al.*[15] These empirical potentials are in reasonable agreement with approximate *ab initio* calculations.[21] Let $\mathbf{q}=q_1,\ldots,q_N$ denote the coordinates of the atoms of the cluster in some fixed frame. To obtain the adiabatic potential surfaces at a given configuration $\mathbf{q}$, we diagonalize the interaction U of Eqs. (2)–(3) (and therefore also the total interaction V of Eq. (1)) in the basis of the orbitals $\{p_x,p_y,p_z\}$, at that configuration:

$$W_i(\mathbf{q})=\mathrm{Diag}_i[\langle p_k|U|p_e\rangle]+\sum_{m>n} u(r_{mn}), \tag{6}$$

where Diag_i denotes the ith diagonal element of the diagonalized interaction matrix. In the Molecular Dynamics method outlined later, the diagonalization is done "on the fly," at each point of the trajectory. Technically, it is convenient to employ the basis $\{ip_x,ip_y,p_z\}$ for real-valued calculations of the matrix elements.

Consider, for instance, the configuration $\mathbf{q}_m$ that corresponds to the minimum energy structure of the cluster in its electronic ground state. The eigenfunctions obtained in the diagonalization will be labeled ξ_1,ξ_2,ξ_3. The angle γ on which they depend can be interpreted to measure the direction vector of the p-electron from the Ba nucleus. It is found that when the atoms are at $\mathbf{q}=\mathbf{q}_m$, then the (adiabatic) orbital $\xi_3(\gamma)$, corresponding to the highest-energy state is a "Σ-type" orbital in the sense that the direction of the orbital points towards the center of the $(Ar)_{125}$ cluster. We write $\xi_1\equiv\xi_{\pi 1},\xi_2\equiv\xi_{\pi 2}$. This classification of the orbitals remains very approximately valid also for configurations $\mathbf{q}\neq\mathbf{q}_m$ reached in the excited state dynamics, although the geometry of $(Ar)_{125}$ deviates then more strongly from that of a sphere. We shall employ this terminology, as done previously by Visticot *et al.*,[15] in discussing the results later on. Note that in general, unlike the case of an atom adsorbed on a perfect sphere, $\xi_{\pi 1}$ and $\xi_{\pi 2}$ are non-degenerate due to local structure effects at the Ba site.

C. Simulations of nonadiabatic dynamics

We apply here a version of the semiclassical surface-hopping method,[2] using the adiabatic states and transitions between them to describe the dynamics. Depending on physical considerations, the surface-hopping method can be applied also to representations that use other electronic basis states, such as diabatic states, and complete the transitions between the latter. In studies of the coupled electronic-nuclear dynamics of F(P) atoms in solid Kr, Krylov and Gerber[22] and Krylov *et al.*[23] used the surface-hopping method to treat transitions between the p_x,p_y,p_z states. In the case of $Ba(P)(Ar)_n$ the adiabatic basis seems a much better one to use: The strong $Ba(P)-Ar$ interactions lead to large energy splittings among the adiabatic states, for most configurations of the system. Therefore it seems reasonable to use the adiabatic states as "zeroth order" states among which (relatively infrequent) transitions take place.

The procedure we follow is similar, although not identical, to the method of Tully.[2] Suppose that initially the system moves on one of the adiabatic potential surfaces $W_i(\mathbf{q})$, where $\mathbf{q}=q_1,\ldots,q_N$. As long as non-adiabatic transitions do not occur, the system is propagated by classical Molecular Dynamics on that surface. At each configuration $\mathbf{q}$, all the adiabatic potential surfaces $W_1(\mathbf{q}),W_2(\mathbf{q}),W_3(\mathbf{q})$ and the corresponding electronic states ξ_i are generated. The adiabatic states $\xi_i(\gamma,\mathbf{q})$ depend parametrically upon the nuclear configuration. Since these states are generated "on the fly" along a trajectory $\mathbf{q}(t)$, we can write $\xi_i\equiv\xi_i(\gamma,t)$ for that trajectory. The electronic degree of freedom is described in this approach by a wavefunction of the coordinate γ only, that evolves in time according to the electronic Schrödinger equation

$$i\,\frac{\partial\psi}{\partial t}\,(\gamma,t)=[H_0(\gamma)+V(\mathbf{q},\gamma)]\psi. \tag{7}$$

$H_0(\gamma)$ is the electronic Hamiltonian associated with the Ba atom, the eigenstates of which are the p-orbitals in our model. V is the nuclear-electronic interaction potential of the cluster, given by Eqs. (1)–(3). The nuclear motions are described by classical trajectories in this approach, so we set $\mathbf{q}=\mathbf{q}(t)\equiv V(q(t),\gamma)$, a time-dependent potential acting on the electronic degree of freedom in Eq. (7). The adiabatic states diagonalize the electronic Hamiltonian on the right hand side of Eq. (7). We expand $\psi(\gamma,t)$ in the adiabatic basis $\xi_j(\gamma,t)$:

$$\psi(\gamma,t)=\sum_{j=1}^{3} C_j(t)\xi_j(\gamma,t). \tag{8}$$

This results in the following equations for the coefficients $C_j(t)$, given by Tully:[2]

$$i\dot{C}_k(t)=-i\sum_j C_j(t)\langle\xi_k|\dot{\xi}_j\rangle+C_k(t)W_k(\mathbf{q}(t)). \tag{9}$$

Using the classical motion of the nuclear coordinates $\mathbf{q}$ ("chain rule"):

$$\left\langle \xi_k\left|\frac{\partial\xi_j}{\partial t}\right.\right\rangle=\dot{\mathbf{q}}(t)\langle\xi_k(\gamma,\mathbf{q})|\nabla_q\xi_j(\gamma,\mathbf{q})\rangle. \tag{10}$$

Applying Hellman–Feynman theorem adiabatic coupling can be calculated analytically (for $k\neq j$):

$$\langle\xi_k(\gamma,\mathbf{q})|\nabla_q\xi_j(\gamma,\mathbf{q})\rangle_\gamma=\frac{\langle\xi_k(\gamma,\mathbf{q})|\nabla_q V(\mathbf{q},\gamma)|\xi_j(\gamma,\mathbf{q})\rangle_\gamma}{W_j(\mathbf{q})-W_k(\mathbf{q})}. \tag{11}$$

$V(\mathbf{q},\gamma)$ in Eq. (7) is the full electronic-nuclear interaction potential of Eqs. (1)–(3), $\dot{\mathbf{q}}$ is the N-dimensional velocity vector of the nuclei. Eqs. (10)–(11) provide a convenient way for analytical evaluating the time-dependent quantities $\langle\xi_k|\dot{\xi}_j\rangle$ which represent the non-adiabatic coupling. These calculations are also done "on the fly." The diagonal elements $\langle\xi_k|\dot{\xi}_k\rangle$ are equal to zero when the adiabatic states are real-valued. In the present case, the adiabatic states can indeed be chosen to be real. Note that the diagonalization procedure, by which the adiabatic states defined here are con-

structed, leaves these states undefined to within a time-dependent phase factor. The choice of phase is necessary for the non-adiabatic coupling equations (9). In the present case, no difficulty arises, and one merely has to ensure that the adiabatic eigenfunctions are continuous in sign. Cases where the basis function are complex valued or when the adiabatic states have an exactly degenerate subset are more complicated, Berry phase problems may arise, and a procedure for construction of the phases is required. This is treated in Ref. 24 in the case of a Cl(P) atom in solid Ar. The algorithm for adiabatic eigenfunction phase treatment will be presented in Ref. 25.

The classical propagation of the nuclei, together with Eqs. (9)–(11) for the electronic state are the basis for the "surface hopping" method. Suppose that initially $C_j(t_0)=1$; $C_k(t_0)=0$ for $k \neq j$. The nuclei are then propagated classically on the adiabatic surface $W_j(\mathbf{q})$. At each point along the trajectory, the adiabatic states all three potential surfaces are constructed, and the non-adiabatic couplings $\langle \xi_k | \dot{\xi}_j \rangle$ are obtained. Eqs. (9) for the coefficients C_l, $l=1,2,3$ are solved numerically, and their variation in time is followed. At sufficiently small time intervals, we test for the possible occurrence of a "surface hopping" event: $|C_k|^2$ is compared with a generated random number $\lambda, 0 \leqslant \lambda < 1$, and on the basis of this stochastic criterion it is decided whether a "hop" from surface j to k has taken place $|C_{k-1}(t)|^2 < \lambda < |C_k(t)|^2$, or not. For stability of the results it was necessary to test for the possible occurrence of hopping each 50 integration steps. In studies examining this point we found that more frequent testing for hopping events does not change the non-adiabatic transition probabilities due to the very small time step ($1–5\times10^{-6}$ ps) employed in the present calculations. This procedure differs from the "minimum number of hops" criterion used by Tully,[2] but our tests indicate that for the present type of system the results of the two should be very similar. Once a hopping event has occurred at some $t=t_1$, we reset the coefficients: $C_k(t_1)=1, C_l(t_1)=0$ for $l \neq k$. The procedure is then continued with the nuclei being propagated on the surface $W_k(\mathbf{q})$. The initial values for the propagation of the trajectory on the new surface are chosen by considerations similar to those discussed by Tully.[2] Eq. (9) for the coefficients is also propagated in time. Very recent tests of Tully's method by Jungwirth and Gerber (7), using Quantum Molecular Dynamics simulations that treat also the nuclear motions quantum mechanically, indicate that the semiclassical results are semiquantitatively very satisfactory, although branching ratios of different electronic states could be off from the quantum MD values by a factor of 2, after about 1.5 ps from the beginning of the process. These tests were for $Ba(Ar)_{10}$, $Ba(Ar)_{20}$, and it is important to pursue the question of the accuracy of the semiclassical method for much larger systems.

In the calculations pertinent to the present study and aimed at comparison with the experiments, the calculations begin with simulations of $Ba(Ar)_{125}$ in the electronic ground state, in thermal equilibrium conditions at $T=35$ K. After equilibration, at randomly chosen time points, the system is promoted vertically to the highest adiabatic energy surface $W_\Sigma(\mathbf{q})$ which, as mentioned previously, corresponds to a Σ-type excitation. The dynamics in time of the system is then followed for 10 ps or more in each trajectory, by the semiclassical, surface-hopping MD simulation. A variety of dynamical properties and spectroscopic quantities are computed as discussed below.

We note that the calculation of the adsorption spectrum was also carried out, by vertical promotion of the configurations from the ground-state MD to the three excited potential surfaces $W_\Sigma(\mathbf{q}), W_{\pi 1}(\mathbf{q}), W_{\pi 2}(\mathbf{q})$. Such a calculation of the adsorption spectrum was already reported by Visticot *et al.*,[15] and is in good accord with the experimental results. The adsorption spectrum does not involve non-adiabatic transitions, and will not be discussed here in detail.

D. Calculation for the polarization of the fluorescence from the semiclassical MD

We now discuss specifically the calculation of the polarization of light emitted from the $Ba(P)(Ar)_n$ cluster, and also of light emitted from excited Ba(P) atoms ejected from the cluster. The comparison of theory and experiment on the polarization is one of the important points in the study, thus the topic merits attention.

We introduce a laboratory fixed coordinate system $\{XYZ\}$, and a second coordinate system $\{xyz\}$ centered in clusters center of mass and with Ba atom on oz-axis [as it is shown on Fig. 7 from Ref. 9]. The transformation from laboratory fixed coordinate system to the body-fixed coordinate $\{xyz\}$ is represented by Euler matrix $\hat{A}(\theta,\phi,\psi)$ which is defined by Euler angles θ,ϕ,ψ. Backward transformation is given by $\hat{A}^T$.

Consider arrangement of the system as in Ref. 9. The excitation light direction is along OX axis while emission is measured in OY direction. Two polarizers are set up in OX and OY directions. One of them can change polarization of excitation light, and the other can filter emission light with an given polarization. When both of are set up parallelly (i.e., extract a light with polarization in OZ-direction), the intensity of the fluorescence with parallel polarization in accordance to excitation light ($I_\parallel$) will be measured. If the orientation of the second polarizer will be changed to the perpendicular one (i.e., to extract light polarized in OX-direction), the intensity of perpendicularly polarized light ($I_\perp$) will be measured. The degree of polarization is defined as:

$$P \equiv \frac{I_\parallel - I_\perp}{I_\parallel + I_\perp}. \tag{12}$$

Let $\vec{\mu}_e$ be the dipole moment for the excitation light, and let $\vec{\mu}_f$ be the dipole moment for emitted light. Denote by ψ_g the ground electronic state of the molecule,by ψ_e the excited electronic state. The intensity of the measured fluorescence for given $\vec{\mu}_e$ and $\vec{\mu}_f$ at time t is given by:

$$I = |\langle \psi_g(t_0) | \vec{\mu}_e | \psi_e(t_0) \rangle|^2 * |\langle \psi_e(t) | \vec{\mu}_f | \psi_g(t) \rangle|^2. \tag{13}$$

In the case of $S \rightarrow P$ transitions, the ground S-state has an spherical symmetry, and the excited state ψ_e is a vector in $\{ip_x, ip_y, p_z\}$-space. The expansion coefficients $\{C_i\}$ for the electronic wave function over the $\{ip_x, ip_y, p_z\}$ basis set determine the orientation of the orbital (defined by the direction of electronic density maximum). Hence, $\psi_e(t)$ can be represented by a vector in a Cartesian coordinates. The orientation of this vector can be extracted from our semiclassical MD-simulation. This yield for the intensities:

$$I = |\vec{\mu}_e \vec{\psi}_e(t_0)|^2 * |\vec{\mu}_f \vec{\psi}_e(t)|^2, \tag{14}$$

where the vector $\vec{\psi}$ is defined by the row of the C_i-coefficients. The expression for polarization calculation can now be written. The coordinates of the $\vec{\psi}$ in laboratory fixed coordinate system are $\hat{A}(\theta,\phi)^T \vec{\psi}$, where θ, ϕ represent the orientation of the cluster in laboratory coordinate system. To describe the random orientations of the clusters, we need to integrate intensity I over all θ, ϕ:

$$I = \int_0^{2\pi} d\phi \int_0^{\pi} \sin(\theta) d\theta (|\vec{\mu}_e \hat{A}(\theta,\phi)^T \vec{\psi}_e(t_0)|^2 * |\vec{\mu}_f \hat{A}(\theta,\phi)^T \vec{\psi}_e(t)|^2). \tag{15}$$

We set now $\vec{\psi}_e(0) = (i,j,k)$, $\vec{\psi}_e(t) = (i(t), j(t), k(t))$, where (i,j,k) are coordinates in the molecular fixed coordinate system. Taking $\mu_e = \vec{Z}$ and $\mu_f = \vec{Z}$ the Eq. (15) yields the intensity of parallelly polarized light $I_\parallel$:

$$I_\parallel = \frac{4(8j^2 j(t)^2 + 2j(t)^2 k^2 + 8jj(t)kk(t) + 2j^2 k(t)^2 + 3k^2 k(t)^2)\pi}{15}. \tag{16}$$

Taking $\mu_e = \vec{Z}$ and $\mu_f = \vec{X}$ Eq. (15) yields $I_\perp$.

$$I_\perp = \frac{2(10i(t)^2 j^2 + 2j^2 j(t)^2 + 5i(t)^2 k^2 + 3j(t)^2 k^2 - 8jj(t)kk(t) + 8j^2 k(t)^2 + 2k^2 k(t)^2)\pi}{15}. \tag{17}$$

Finally,

$$P = \frac{-10i(t)^2 j^2 + 14j^2 j(t)^2 - 5i(t)^2 k^2 + j(t)^2 k^2 + 24jj(t)kk(t) - 4j^2 k(t)^2 + 4k^2 k(t)^2}{10i(t)^2 j^2 + 18j^2 j(t)^2 + 5i(t)^2 k^2 + 7j(t)^2 k^2 + 8jj(t)kk(t) + 12j^2 k(t)^2 + 8k^2 k(t)^2}. \tag{18}$$

The maximum possible parallel polarization $I_\parallel = 1/2$ (it corresponds to the case when there is no changes in excited state after excitation). The maximum value for perpendicular polarization $I_\perp = -1/3$ (it corresponds to the situation when the excited state changes its orientation to the pure perpendicular one).

III. EXPERIMENT

A. Experimental approach

The basic experimental set-up has been previously described in detail.[8,9] A beam of neutral argon clusters is generated by a supersonic beam source. The mean size of the clusters is varied from $\langle N \rangle = 3 \cdot 10^2$ to $4 \cdot 10^3$ by changing the argon stagnation pressure in the source. The cluster size measurements are performed directly on the experimental set-up by the slow-down technique (10) and by a Rayleigh scattering experiment (11) with a relative accuracy of 10% and an absolute uncertainty of 50%.

After being skimmed, the argon cluster beam flies horizontally through a cell that contains a barium vapor. Collisions between argon clusters and barium atoms result in a collisional attachment of barium atoms to the cluster. The barium pressure is adjusted so that the argon clusters never contain more than one barium atom.

Finally, the clusters cross the excitation zone, where they are illuminated by the light of a tunable cw ring dye laser, whose wavelength can be tuned between 527 and 550 nm. The laser light crosses the cluster beam vertically. In part of the experiment reported below, the laser polarization is controlled and can be rotated about the laser light axis.

The fluorescence emission of the central part of the irradiated zone is collected and focused onto the entrance slit of a scanning grating monochromator, before detection by a photomultiplier tube and storage in a PC-computer. The resolution of the monochromator is about 0.5 nm. The axis of collection lies in the horizontal plane and a polarizer selects the polarization component of the emission in the same plane.

B. Experimental results

The experimental set-up allows three types of experiment to be performed.

- Fluorescence spectra. They are obtained by fixing the laser frequency and scanning the monochromator wavelength.
- Excitation spectra. They are recorded by scanning the laser frequency either at a fixed monochromator wavelength or by recording the undispersed fluorescence.
- Polarization measurements. They consist in fixing both the monochromator and the laser wavelengths and rotating the direction of polarization of the laser.

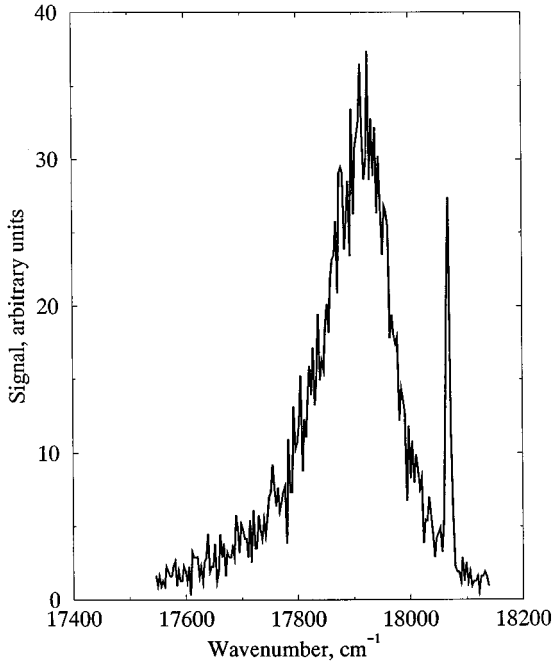

FIG. 1. Measured fluorescence following the photoexcitation of $BaAr_{300}$ clusters at 540.3 nm.

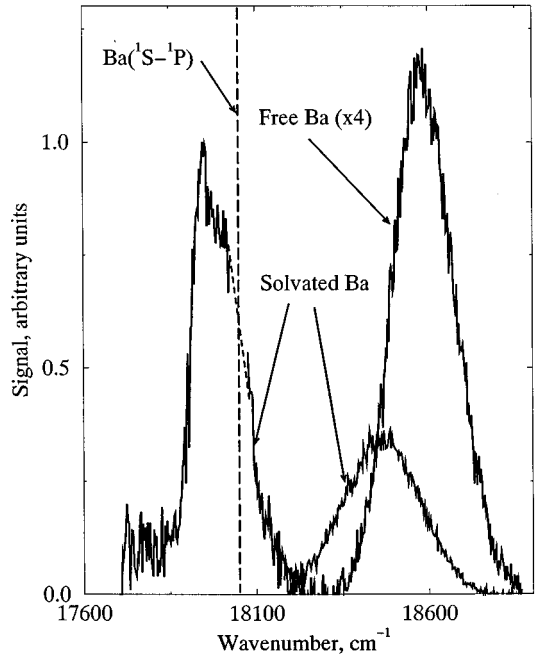

FIG. 2. Experimental excitation of the $BaAr_{300}$ clusters. The left spectrum (labeled solvated barium) was measured with the monochromator set to the maximum of the broad feature of the fluorescence spectrum, i.e. it shows the excitation spectrum of the solvated barium barium fluorescence. The right spectrum (labeled free barium) corresponds to the monochromator set to the emission of free barium. It thus shows the excitation spectrum of the free barium fluorescence for those barium atoms that are attached to the argon cluster prior to the laser excitation. The dashed line indicates the position of the $6s^2\,{}^1S_0 \rightarrow 6s6p\,{}^1P_1$ transition of free barium atoms.

Experimental results obtained along these lines have already appeared in the literature. Their interpretation has provided a first insight into the dynamics of electronically excited barium atoms within the cluster environment.[8,12–15] These results are reviewed hereafter, since they provide the framework for which the present Molecular Dynamics calculations have been developed, and offer a critical tests of the theoretical method presented here.

In view of the comparison with the present calculations performed for clusters of 125 argon atoms, all the quantitative experimental results reported below correspond to the smallest clusters we could investigate experimentally, i.e. clusters of an average size of 300 atoms with a full-width at half-maximum of 300. Since several of the previously published experiments have been run with larger clusters, we have performed a few experiments again in order to have a complete set of experimental data for the Ar_{300} clusters.

C. Fluorescence spectra

A typical fluorescence spectrum is shown in figure 1 for an excitation wavelength of 540.3 nm. The spectrum is composed of a narrow line superimposed to a broad feature.

The narrow line is the resonance line $6s^2\,{}^1S_0 \leftarrow 6s6p\,{}^1P_1$ of the cluster excited by the 540.3 nm laser light. These atoms have desorbed from the cluster before electronic de-excitation and fluoresce as free atoms. This phenomenon has been investigated in Ref. 9. It exists when the excitation wavelength is smaller than 545 nm. It is examined in further detail in this study.

The broad feature of the spectrum has been assigned to the emission of barium atoms that stay adsorbed on the cluster after excitation by the laser and are relaxed to the most stable excited configuration (12), (15).

D. Excitation spectra

For each type of fluorescence identified above a measurement of the corresponding excitation spectrum was required. The resulting two excitation spectra are shown in figure 2.

The excitation spectrum for the fluorescence of free barium was recorded with the monochromator set to the emission of free barium at 553.5 nm. It features a broad band of 200 cm^{-1} FWHM centered at 18580 cm^{-1}. The excitation spectrum of the solvated barium emission has two main bands:

• A blue one that overlaps the excitation spectrum for the fluorescence of free barium. For these reasons, the fluorescence has been dispersed and the blue band of the excitation spectrum has been measured with the monochromator set to the maximum of the broad feature of the fluorescence spectrum (the one that is assigned to the fluorescence of solvated barium). This band of the excitation spectrum has a 300 cm^{-1} width. It is centered at 18450 cm^{-1}. It has been observed that the shape of this band does not change when switching the detection from dispersed fluorescence as shown in figure 2 to undispersed fluorescence. This is an indication that the channel leading to the free barium emis-

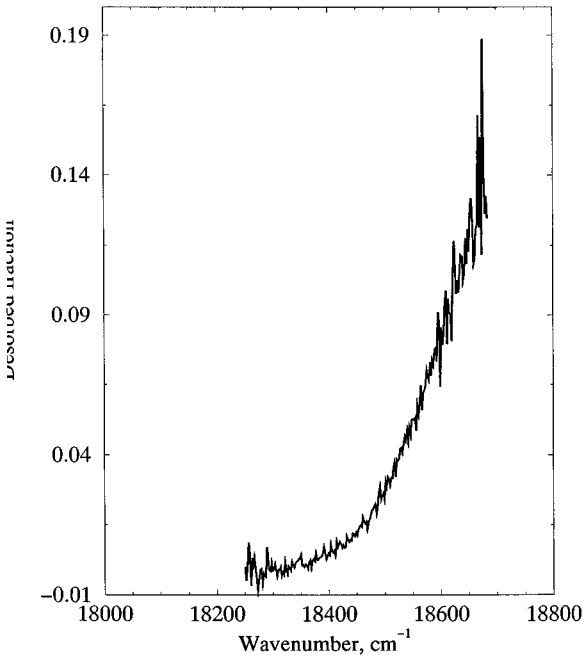

FIG. 3. Measured fraction of excited barium atoms desorbed off Ar_{300} clusters as a function of the wavenumber of the excitation light.

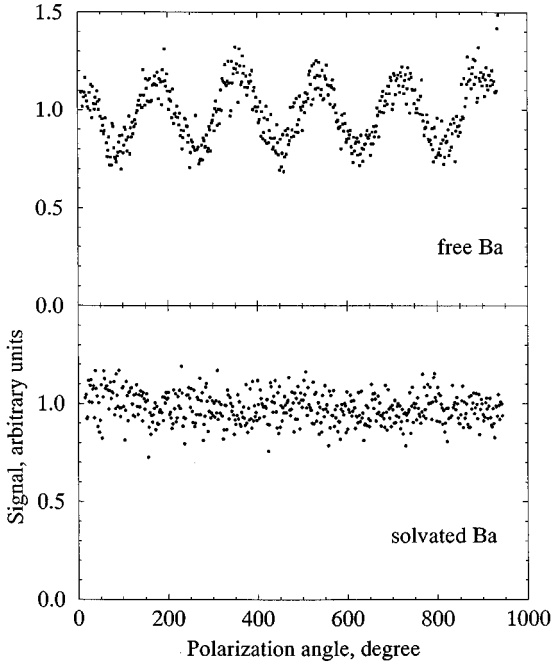

FIG. 4. Measured polarization effect in the photoexcitation of $BaAr_{300}$ clusters at 540.3 nm. The figure shows the variation of the fluorescence intensity of free and solvated barium with the angle that the polarization direction of the fluorescence light makes with that of the excitation light. An angle of 0° corresponds to parallel directions.

sion is minor compared to that leading to the solvated emission. We shall come back to this point later on.

• The excitation spectrum has a red band that does not overlap the excitation spectrum of free barium. For this reason, it has been measured by recording the undispersed fluorescence. In this way we are sure that the detection procedure does not introduce a bias due to small shifts of the fluorescence spectrum when the excitation wavelength is varied.

A careful analysis reported in Ref. 9 has allowed us to report the fraction of barium atom that desorb off the cluster upon laser excitation. It is shown in figure 3 as a function of the wavenumber of the excitation laser. The desorbed fraction increases as the energy of the excitation photons is increased. It never exceeds 20% in the domain of photon energy that was explored. The range of photon energy over which this curve can be explored is actually limited by the fact that these photons must be within the excitation spectrum of free barium (see figure 2), i.e. within the range 18250–18700 cm^{-1}.

The excitation spectrum of solvated barium shown in figure 2 has been interpreted semiquantitatively by a Molecular Dynamics simulation[15] and the calculations were repeated in the framework of the present study. The main result of the calculations is that ground state barium is solvated at the surface of the cluster. The splitting of the excitation into two bands, one shifted to the blue and the other shifted to the red of the barium resonance line has been interpreted as a print of the nearly cylindrical environment of surface solvated barium. Within this picture, the blue component appears as a Σ-like absorption of the Ba-Cluster complex, whereas the red one is a Π-like absorption. Only the Σ-like absorption leads to a minor desorption channel of barium.

E. Polarization measurements

The polarization of the fluorescence light was measured by rotating the laser beam polarization with both the laser wavelength tuned to the Σ-like absorption at 540.3 nm and the monochromator wavelength kept either to the free barium fluorescence line at 553.5 nm (upper part of figure 4), or tuned to the maximum of the broad emission of solvated barium at 558 nm (lower part of figure 4). In this experiment, a polarizer is placed in the horizontal plane in front of the monochromator that disperses the fluorescence light. A polarization angle of 0° corresponds to a parallel alignment of the laser polarization with the fluorescence polarization that is detected.

As can be seen from figure 4, the modulation of the free barium signal is in phase with the rotation of the polarizer, i.e. the signal is maximum when the light is polarized parallel to the detected polarizer and minimum for the perpendicular direction. Defining the degree of polarization by $P=(I_{\parallel}-I_{\perp})/(I_{\parallel}+I_{\perp})$ the observation of figure 4 corresponds to a positive degree of polarization. It has been extensively measured in Ref. 9. A value of $21\pm2.5\%$ has been found with no significant dependence on the excitation wavelength or on the cluster size. This value is about half that expected for a direct photodesorption that preserves the initial Σ-like alignment of the excited $6p$ orbital of barium. Various origins of depolarization have been discussed in Ref. 9. It has been suggested that the barium desorption is not a

direct process. A further indication in that sense has emerged in the same work when discussing energy thresholds such as that shown in figure 3 for the desorption of barium. It has been necessary to propose that some of the cluster potential energy is transferred to the barium to allow its desorption. This energy would correspond to the rearrangement of the cluster argon atoms that proceeds simultaneously with the desorbtion of barium from the cluster. The desorption of Ba atoms and the polarization of emitted light from these atoms will be extensively discussed and interpreted on the basis of the simulations carried out in the recent work.

The modulation of the captured barium fluorescence is shown in the lower panel of figure 4. It is very small and cannot be determined with the clusters of size 300 because of too low signals. It has been determined for larger cluster sizes in Ref. 9. A negative value of $-5\pm3\%$ was found. It indicates that fluorescence of solvated barium has a slight maximum when the incident radiation is polarized perpendicularly to the detection polarizer. This result shows that the initial Σ-like excited orbital of barium did an average rotation of 90°. Barium thus stays solvated with a Π-like excited orbital before it emits the fluorescence light. However, much polarization scrambling occurs within the solvation medium and gives a very wide distribution to the alignment direction of the excited orbital. Again, providing a detailed quantitative interpretation of the polarization of the light emitted from the $Ba(P)(Ar)_n$ clusters is a key objective of the theoretical studies here, and will be discussed in the next section.

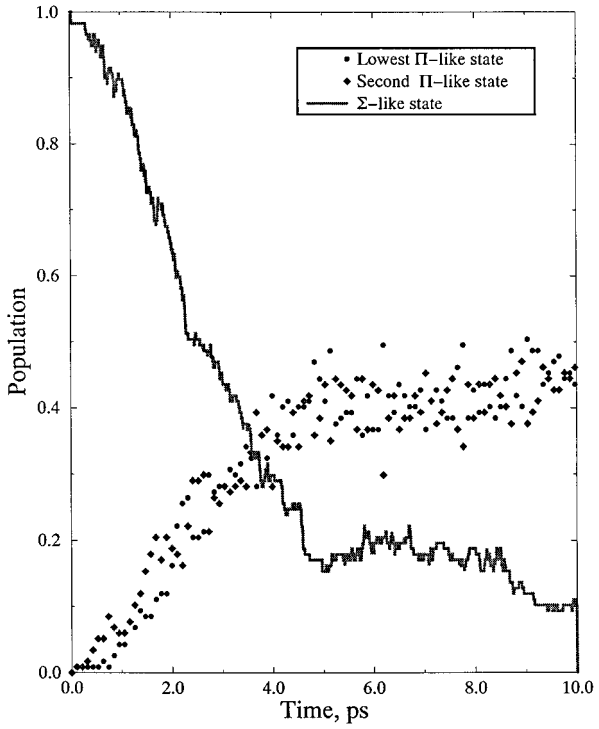

FIG. 5. Calculated populations of electronic states of $Ba(P)(Ar)_{125}$ versus time (solid line): Σ-state; (circles): $\Pi 2$-state; (diamonds): $\Pi 1$-state.

IV. SIMULATION RESULTS, COMPARISON WITH EXPERIMENTS AND DISCUSSION

The photoexcitation dynamics results discussed here are from the Molecular Dynamics simulations including ''surface hopping'' described in Sec. II. 100 trajectories were calculated for $Ba(Ar)_{125}$, corresponding to initial cluster temperature $T=35$ K. Simulations were also carried out for $T=70$ K, and show no major differences. Each P-state trajectory was propagated for 10 ps or more. It will be useful below to organize the discussions around several main findings.

A. Electron relaxation dynamics

The total energy of the cluster upon excitation to the Σ-type state and at the temperature of the study suffices for the ''evaporation'' of the Ba(P) atom, or of an argon atom. However, this did not occur in any of the trajectories. Rather, the excitation energy was found, on an initial time-scale of 1–2 ps, to undergo rapid redistribution among cluster vibrational modes. On a qualitative level, inspection of the trajectories shows that part of the redistribution seems ''statistical'' in character, but also part of the excitation seems to travel as a shock wave in the Ar ''microcrystal.'' From our point of view, the most important facts are: (i) There is no direct, immediate ejection of a Ba atom (or of an Ar) upon photoexcitation; (ii) The initial impulse of excitation leads to vibrational energy redistribution in the cluster, which is already extensive within 1–2 ps. The larger-amplitude motions in the excited cluster are favorable to electronic transitions between the potential surfaces of the P-state manifold. The populations of the three adiabatic electronic states versus time are shown in figure 5. As seen from the figure, during the first 10 ps following excitation, 90% of the population relax to the Π-states. An exponential fit $e^{-t/\tau}$ to the initial decay of the Σ-state population yields $\tau=4.4$ ps. After fast initial decay the electronic relaxation rate slows down. A plausible explanation of vibrational energy in the cluster, the local site of the Ba atom becomes less ''hot,'' and the local ''collisions'' between the Ba and the neighboring Ar atoms are increasingly less energetic, which decreases the rate of electronic transitions. The two Π-type states are nearly degenerate and their populations are almost identical. The relaxation is not completely over even after 10 ps. This could be due to the large mass of the Ba atom, as a result of which its vibration cooling may be slow, with a corresponding effect on the electronic-vibrational transitions. Figure 6 shows results of the decay of the Σ-state population for $Ba(Ar)_{125}$ initially at 70 K, compared with the calculations for the cluster at 30 K. The initial electronic decay at 70 K is appreciably faster ($\tau = 2.5$ ps versus $\tau=4.4$ ps for the case of $T=30$ K). However, after 5 ps the Σ-state populations in the two cases are very similar. Given the fact that vibrational energy redistribution at 5 ps has already progressed to a nearly complete stage the long time behavior in figure 6 is intuitively expected. The main finding from figures 5 and 6 is that the initial electronic relaxation in this system is very fast—of the order of several picoseconds. This result is very important for the interpretation of the experiments. The electronic relaxation is much

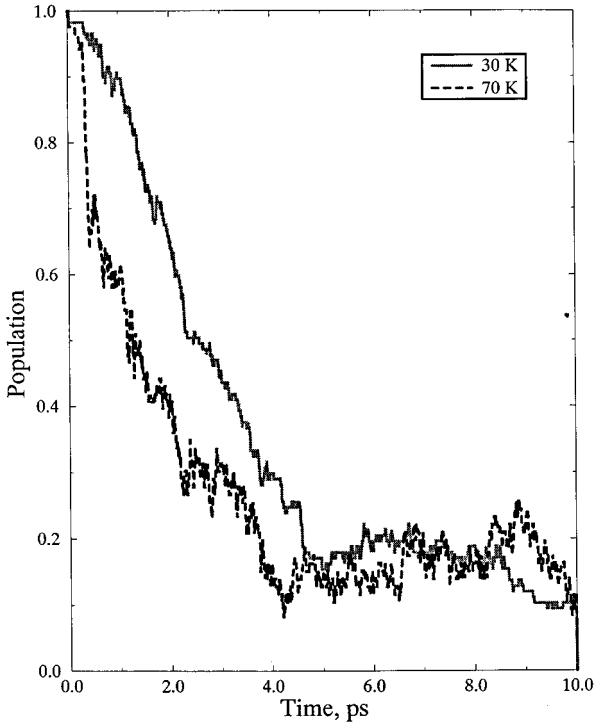

FIG. 6. Calculated decay in time of Σ-state population of $Ba(Ar)_{125}$. The curves shown are for initial cluster temperatures of 30 K and 70 K, respectively.

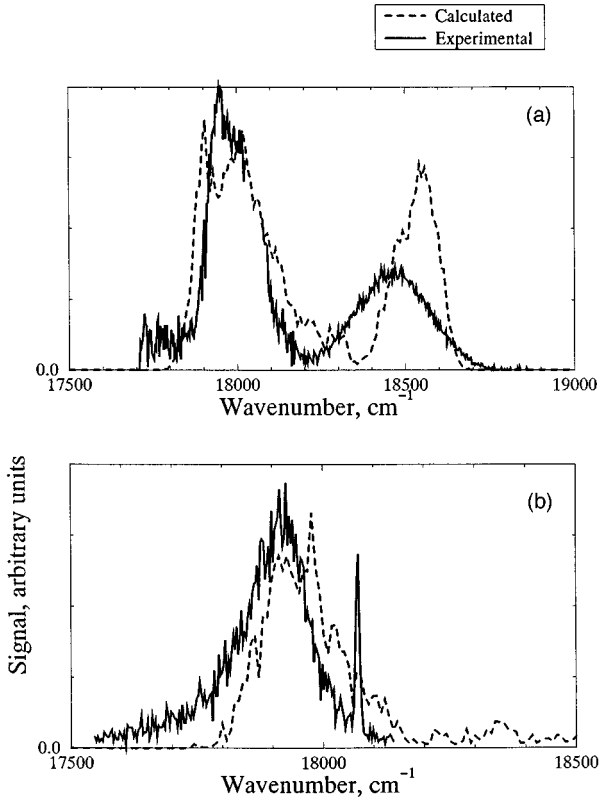

FIG. 7. (a) The calculated excitation of $Ba(Ar)_{125}$, compared with the experimental result. (b) The calculated emission spectrum of $Ba(Ar)_{125}$, compared with the experimental result.

faster here than the time-scale for radiative emission, implying that the emission spectrum should come almost totally from the Π-states. This, indeed, is in accord with the observations both for the emission band shape and for the polarization of the radiation from the cluster. Also, the initial electronic relaxation is much faster than the ''evaporation'' rate of Ba atoms from the clusters. The binding of the Ba atom to the cluster is much stronger in the Π-states. It follows that Ba atoms are most probably ejected from the cluster in a Σ-state, but only after having a previous ''history'' in the Π-state. As we shall see, non-adiabatic $\Pi \rightarrow \Sigma$ transitions can take place in the cluster when a dynamical fluctuation brings sufficient vibrational energy and momentum to the Ba, but this is an event of very low probability, and it occurs in a long delay after the initial excitation. Again, these facts are in accord with the experimental data and deductions made.

B. Emission spectrum and polarization of radiation from $Ba(P)(Ar)_{125}$ cluster

As follows from the above results on the Σ-state population decay, almost all the emission is from the $\Pi 1$ and $\Pi 2$ states. In our simulations, after 10 ps about 10% of unrelaxed emission was obtained. Most of the emission in the experiment comes, however, after a much longer time (order of nanoseconds). The amount of unrelaxed emission is then expected to have many more modes than in our calculations, but some such emissions can take place, especially if we keep in mind that after 5–10 ps the electronic relaxation rate seems to go down. In the calculations of the emission spectrum at any given time t, we projected in a Franck-Condon manner the excited state configurations for each of the trajectories at that time onto the S-state potential surface. The projection is applied regardless of which excited state adiabatic potential surface the system is at for the given time.

Figure 7 shows the excitation spectrum of $Ba(S) \times (Ar)_{125}$, and the emission spectrum of $Ba(P)(Ar)_{125}$ calculated at $t=10$ ps after the excitation. The results are compared with the experimental spectrum. One must, of course, keep in mind that the real radiative lifetime is much longer than 10 ps. The agreement between experiment and theory is very good. The most important feature is that the emission spectrum is shifted to the red compared with the excitation spectrum, also shown in figure 7. This shift is due to the fact that the emission takes place after the system was largely relaxed electronically to the Π-states, and after the vibrational state distribution has undergone almost complete equilibration within these states. It can safely be assumed that for larger simulations in the P-state manifold the relaxation will be more complete, and the emission spectrum computed will be more red-shifted. The quantitative difference between the theoretical and experimental emission spectra is important, and the possible origins of the discrepancy deserve attention. We estimate that the quantitative differences between theory and experiment stem from the following causes: (i) Insufficient accuracy of the interaction potentials. The major importance of this factor can be seen

from the fact that there is also a discrepancy of roughly similar magnitude between the measured and computed adsorption spectra (for which relaxation dynamics does not play a role). (ii) The fact that the experimental system corresponds to a size distribution of clusters; and the mean size is indeed larger than the theoretical model used, $Ba(Ar)_{125}$. We argued that for $n \geqslant 125$, most effects are probably already size independent, but this may not hold on a full quantitative level. In our assessment this factor is less important than the issue of the potentials mentioned above. (iii) The fact that the theoretical excited state simulations were only pursued to about 10 ps, while the real emission time is in the nanosecond range. This certainly plays some role in the discrepancy, since the electronic state population is not completely relaxed (about 90%) at the time when the emission calculation is carried out. A factor which in our estimate *does not* play a significant role with regard to the partial discrepancy with experiment is the dynamical ''surface hopping'' method. Quantum dynamics simulations by Jungwirth and Gerber for $Ba(Ar)_{10}$, $Ba(Ar)_{20}$ show that electronic state populations calculated by the semiclassical ''surface hopping'' approach, are in quantitative error by a factor of the order of 2 over a time interval of about 1 ps.[7] However, the emission timescale for the present cluster is, as mentioned, in the nanosecond range. It seems likely that for such times both the semiclassical and the quantum calculations, had they been done, would have yielded a similar, fully relaxed electronic state distribution. In summary of this point we stress that given the complexity of the system, overall the agreement between theory and experiment is a very satisfactory one, and sufficient to support semiquantitative conclusions on the dynamics. For much more demanding tests of the relaxation dynamics, it is very desirable to have ultrafast, time-resolved spectroscopic experiments. Such experiments are not yet available for our type of system, but to predict the behavior we calculated the *time—resolved emission spectrum* of the system. The emission spectrum in time intervals of 1 ps is shown in figure 8. An evolution in stages of the spectrum is seen. Over the first picosecond, hardly any electronic state has set in, and the emission from the Σ-state dominates. The effect of electronic relaxation becomes noticeable for the spectrum calculated for the 1–2 ps time interval. As the results show, at later times the evolution of the emission spectrum slows down. This, of course, is an indication of the slowing down of the relaxation process for $t \gtrsim 5$ ps, mentioned earlier. As these results show, time-domain experiments with sub-picosecond time resolution, and extending over about 10 ps should be rich in dynamical information.

Same as the emission spectrum, so is the polarization of the emitted radiation governed by the excited-state relaxation. The calculated time-dependent emission from $Ba(P) \times (Ar)_{125}$ is shown in figure 9 (curve labeled solvated Ba). During the relaxation process, the polarization of the emission changes from a parallel one to a nearly perpendicular one. The deviation of the polarization from the pure perpendicular value (-0.33) is due to the fact that the p-orbital orientation for the adiabatic excited states is not exactly ''parallel'' or ''perpendicular'' but quite broadly distributed.

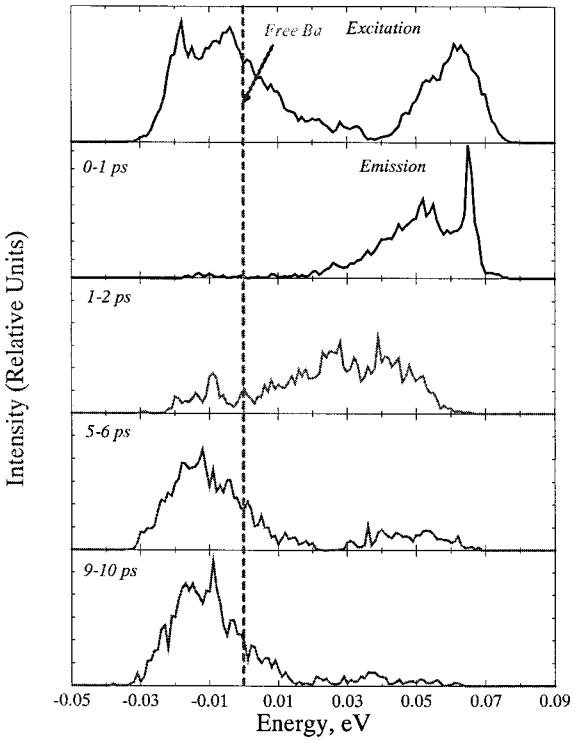

FIG. 8. The calculated evolution of emission spectrum from $Ba(P)(Ar)_{125}$ in time. The excitation spectrum is also shown. $j-(j+1)$ ps indicates emission spectrum calculated between j ps and $(j+1)$ ps after excitation.

The distributions of the p-orbital orientation for the Σ and Π types of states is shown in figure 10. Note that the θ distribution of the orientations is wide for both the Σ and the Π states. The Π states are clearly not exactly normal to the

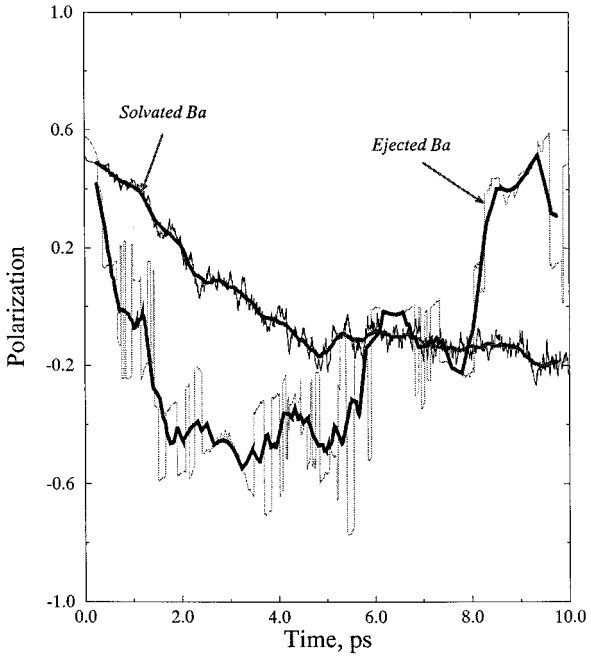

FIG. 9. The calculated evolution in time of the polarization of emitted radiation. Polarization of light from $Ba(P)(Ar)_{125}$ and from Ba(P) atoms ejected from the cluster are shown by separate curves.

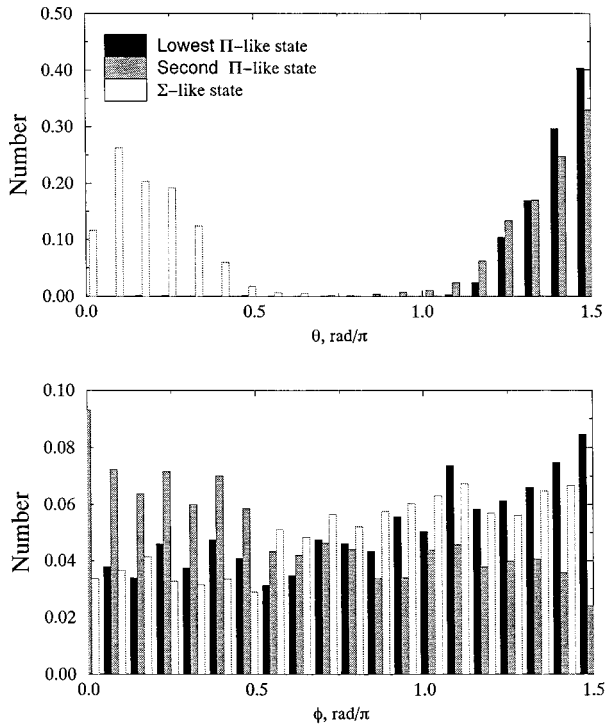

FIG. 10. Calculated distribution of orbital orientation in the Σ-type and Π-type adiabatic states of $Ba(P)(Ar)_{125}$. Upper part: θ-angle distribution. Lower part: ϕ-distribution.

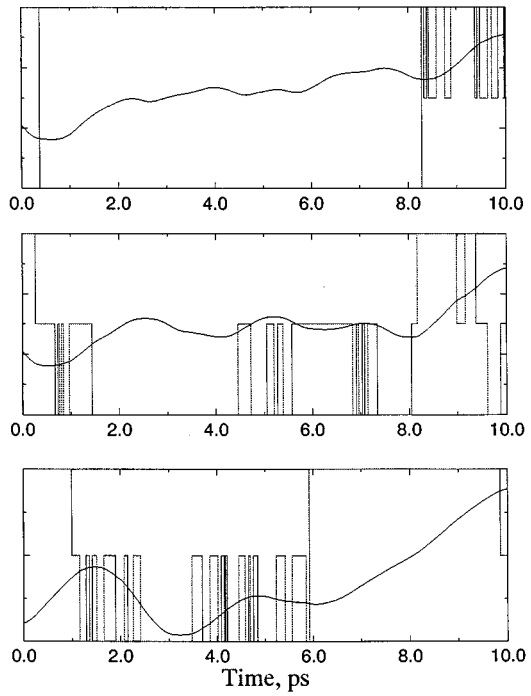

FIG. 11. Trajectories resulting in evaporation of Ba(P) atoms from the cluster. For each of the trajectories, the distance of Ba from the cluster is shown. The horizontal lines give the electronic state of the system along the trajectory. Highest level indicates Σ-state. The second level is for the $\Pi 2$-state, and the lowest is for $\Pi 1$. (The scale is not quantitative in energy.)

orientation of the initially-prepared Σ-type excitation. Hence the smaller value of the polarization found. Going back to figure 9, we note that the polarization of radiation from the cluster evolves almost monotonically in time, falling off as relaxation progresses. Our simulations shows that 10 ps after photoexcitation the polarization is about -15%. Hence, the calculated polarization of the solvated Ba emission has more perpendicular character than the experimental one ($-5 \pm 3\%$). There are two reasons for the discrepancy: more complete relaxation of the Ba atoms on the nanosecond timescale of the present experiment and possible migration of the Ba atoms on the cluster surface or slow rotation of the clusters. The latter processes also occur on the nanosecond timescale, hence, they can not be reproduced in the short time simulations. With these reservations kept in mind, we conclude that the calculated polarization of the fluorescence is in good semiquantitative accord with the experimental result, and supports the interpretation that for that time and beyond the cluster has largely relaxed to the Π-states.

C. Ejection of Ba(P) atoms from the cluster, and the polarization of the atoms

The mechanism whereby Ba(P) atoms are ''evaporated'' from the cluster, and the polarization of radiation these atoms emit, is amongst the most interesting aspects of the excited state dynamics. By the results of previous sub-sections, it is clear that direct, impulsive ejection of a Ba(P) atom upon photoexcitation does not take place in the simulations. The initial impulse of excitation is transferred as vibrational energy into the Ar cluster. Then, electronic energy relaxation sets in—it is faster than the time-scale for Ba atom ejection. In the Π-states, the binding energy of the Ba atom to the cluster is stronger. Indeed, our simulations show that after trapping, as relaxation progresses, the energy spacing between the Π-states and the Σ-state increases, making the back-transition into the Σ (from which evaporation is more probable) a less likely event. Nevertheless, in our calculations 3 trajectories out of the computed 100 at 30 K yielded Ba(P) evaporation. The ''history'' of these ejection events is shown in figure 11. The figure shows the distance of the Ba atom from the cluster versus time along each trajectory. Also shown is the electronic state of the system along the trajectory. In all three cases the system was first trapped in the Π-states. Evaporation was a very delayed event in the three cases. It resulted from the fact that non-adiabatic transitions, including $\Pi \rightarrow \Sigma$ transitions do occur in the cluster, although the probability of the latter is very small. In all three cases of evaporation shown in figure 10, at the critical moment of release from the cluster the Ba atom was in the Σ-type state. (At very large distances of the Ba atom from the cluster, after the escape, the Σ and Π energies are the same.) Figure 12 shows the potential energy of the system in the Σ and in the Π-states along some trajectory. The time-averaged splitting between the Σ and Π potential energies is around 0.03 eV, but there are points where the difference is only 0.01 eV or less. The Boltzmann probability of being in the excited state at such points is around 5%. This means that for the Ba atom to jump back to the Σ-state is not an event of completely

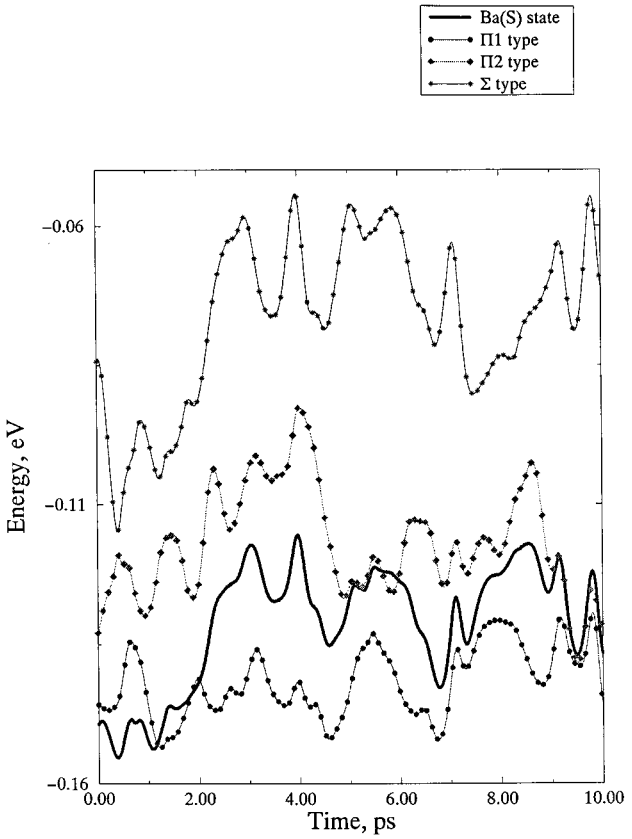

FIG. 12. Potential energy versus time of the ground $Ba(S)Ar_{125}$-state (solid line), Σ (stars), $\Pi 2$ (diamonds) and $\Pi 1$ (circles) potential surfaces along a specific trajectory.

negligible probability. Also, when the Π-states are populated, the cluster is hotter, and the extra kinetic energy is favorable to the transition. We are not certain whether the $\Pi \rightarrow \Sigma$ jumps we saw are essentially statistical, or whether a ''shock wave'' excitation by the hot vibrations of the cluster play a role. When the $\Pi \rightarrow \Sigma$ transition occurs it is still necessary for the Ar atoms at the Ba site to have the right direction of momenta for ejection to occur. This condition, not fulfilled in the excited case, is indeed satisfied for the trajectories described in figure 10. Since the ejection takes place when the system makes a back transition to the Σ-state, the polarization of the ejected Ba atoms is parallel. The polarization for the trajectories ultimately resulting in Ba ejection versus time is shown in figure 9. Evidently the polarization history of these trajectories is not monotonic. The time dependence shows they first were trapped in the Π-state (that is when the computed polarization went down), but upon ejection they had a Π-state polarization. The calculated evaporation yield of a few percent is at least in semiquantitative agreement with experiment (see figure 3). Likewise, the calculated polarization of the ejected Ba atom agrees well with experiment. This, in our opinion, strongly supports the ejection dynamics proposed here.

D. Cluster size effects

Our comments on this point are based not on comparison between theory and experiment, but on comparison between the present results and recent simulations by Jungwirth and Gerber on the much smaller clusters $Ba(Ar)_{10}$,$Ba(Ar)_{20}$.[7] The photoexcitation dynamics of $Ba(Ar)_{10}$ is qualitatively different from that of the present $Ba(Ar)_{125}$. The main difference lies in the fact that direct ejection of Ba(P) upon excitation is the dominant channel in $Ba(Ar)_{10}$. The yield for this is $\sim 80\%$.[7] Due to the small number of Ar atoms, the binding of Ba to the cluster in $Ba(Ar)_{10}$ is much smaller than in the system studied here. Also, the efficiency of energy redistribution in the cluster following photoexcitation is low in the small $Ba(P)(Ar)_{10}$. The probability of non-adiabatic transitions in the clusters that do not undergo evaporation is actually high, since the excited small cluster is very ''hot,'' but overall the channel resulting in Ba ejection dominates. In $Ba(Ar)_{20}$ already notes a transition to behavior similar to the one found here: The direct photoinduced evaporation has a yield of 20% only. Non-adiabatic transitions are slower in absolute rate than for $Ba(Ar)_{10}$, but are relatively more important in the dynamics since most clusters survive the photoexcitation. The timescales and mechanisms of the non-adiabatic transitions are similar to the ones found here. All this suggests that the regime of small clusters, $Ba(Ar)_n$ with $10 \leqslant n \leqslant 20$ should be a highly interesting one to explore experimentally, as this is the size range where the crossover to large cluster behavior begins.

V. CONCLUDING REMARKS

In this paper a combined theoretical and experimental study was made of the non-adiabatic dynamics of photoexcited Ba atoms adsorbed on the surface of large argon clusters. The results, and the comparison between simulations and experiment, lead to a coherent picture of the dynamical processes involved and the mechanisms whereby they occur. One of the main findings is that electronic relaxation is very efficient in this system, setting in effectively already for $t \approx 2$ ps, and being largely complete by $t = 10$ ps, although it slows down for $t > 5$ ps. The initial impulse of excitation is converted to vibrational energy of the cluster, and the large amplitude motions and high energy trigger the non-adiabatic processes. The rapid electronic relaxation within the P-state manifold determines the emission spectrum from the cluster, and the polarization of the emitted radiation. Ba atoms are not ejected directly from the cluster upon photoexcitation. Trapped in the more attractive Π-states after electronic relaxation, Ba atoms are ejected only with very low probability, and after considerable time delay. The ejection mechanism involves a non-adiabatic $\Pi \rightarrow \Sigma$ back transition, which can occur when a dynamical fluctuation brings vibrational energy and momentum to the site of the Ba atom.

The agreement found here between the semiclassical ''surface hopping'' simulations and experiment is semiquantitatively very good, lending support for the use of this method in studying non-adiabatic transitions in condensed phases. At the same time, the tests applied here for the method were not the most demanding. Sub-picosecond time-domain spectroscopic experiments could, for instance, provide a more stringent and quantitative test of the method.

This, and other types of further experiments are strongly needed to forge a more quantitative and rigorous understanding of non-adiabatic dynamics in extended systems.

ACKNOWLEDGMENTS

J.P.V. and J.M.M. acknowledge P. de Pujo for fruitful discussions. R.B.G. and A.I.K. thank Dr. Pavel Jungwirth for useful discussions. A.I.K. thanks Mr. L. Ya Baranov for very stimulating and useful discussions. This research was supported in part by a grant (to R.B.G.) from the Israel Science Foundation, operated by the Israel Academy of Sciences. The part of this research done at U.C. Irvine was supported in part by a grant from the Chemistry Division of the NSF.

[1] J. C. Tully and R. K. Preston, J. Chem. Phys. **55**, 562 (1971).
[2] J. C. Tully, J. Chem. Phys. **93**, 1061 (1990).
[3] P. J. Kuntz, J. Chem. Phys. **95**, 141 (1991).
[4] F. Webster, E. T. Wang, P. J. Rossky, and R. A. Freisner, J. Chem. Phys. **100**, 4835 (1994).
[5] D. F. Coker, J. Chem. Phys. **102**, 496 (1995).
[6] H.-D. Meyer and W. H. Miller, J. Chem. Phys. **70**, 3214 (1979).
[7] P. Jungwirth and R. B. Gerber, J. Chem. Phys. (in press).
[8] A. Lallement, J.-M. Mestdagh, P. Meynadier, P. de Pujo, O. Sublemontier, J.-P. Visticot, J. Berlande, X. Biquard, J. Cuvellier, and G.G. Hickman, J. Chem. Phys. **99**, 8705 (1993).
[9] B. Schilling, M.-A. Gaveau, O. Sublemontier, J.-M. Mestdagh, J.-P. Visticot, X. Biquard, and J. Berlande, J. Chem. Phys. **101**, 5772 (1994).
[10] J. Cuvellier, P. Meynadier, P. de Pujo, O. Sublemontier, J.-P. Visticot, J. Berlande, A. Lallement, and J.-M. Mestdagh, Z. Phys. D **21**, 265 (1991).
[11] A. J. Bell, J.-M. Mestdagh, J. Berlande, X. Biquard, J. Cuvellier, A. Lallement, P. Meynadier, O. Sublemontier, and J.-P. Visticot, J. Phys. D **26**, 994 (1993).
[12] J.-P. Visticot, J. Berlande, J. Cuvellier, A. Lallement, J.-M. Mestdagh, P. Meynadier, P. de Pujo, and O. Sublemontier, Chem. Phys. Lett. **191**, 107 (1992).
[13] P. de Pujo, J.-M. Mestdagh, J.-P. Visticot, J. Cuvellier, P. Meynadier, O. Sublemontier, A. Lallement, and J. Berlande, Z. Phys. D **25**, 357 (1993).
[14] J.-M. Mestdagh, A. J. Bell, J. Berlande, X. Biquard, M. A. Gaveau, A. Lallement, O. Sublemontier, and J.-P. Visticot, in *Proceedings of the 26th Jerusalem Symposium on Quantum Chemistry*, edited by J. Jortner, R. D. Levine, and B. Pullman (Kluwer, Dordrecht, 1994), p. 101.
[15] J.-P. Visticot, P. de Pujo, J.-M. Mestdagh, A. Lallement, J. Berlande, O. Sublemontier, P. Meynadier, and J. Cuvellier, J. Chem. Phys. **100**, 158 (1994).
[16] M. P. Allen and D. J. Tildesley, *Computer Simulations of Liquids* (Clarendon, Oxford, 1987).
[17] R. A. Aziz and M. J. Slaman, Mol. Phys. **58**, 679 (1986).
[18] F. O. Ellison, J. Am. Chem. Soc. **85**, 3540 (1963).
[19] C. H. Becker, P. Cassavecchia, and Y. T. Lee, J. Chem. Phys. **70**, 5477 (1979).
[20] V. Aquilanti, G. Liuti, F. Pirani, and F. Vecchicattivi, J. Chem. Soc. Faraday Trans. **85**, 955 (1989).
[21] E. Czuchaj (unpublished).
[22] A. I. Krylov and R. B. Gerber, Chem. Phys. Lett. **231**, 395 (1994).
[23] A. I. Krylov, R. B. Gerber, and V. A. Apkarian, Chem. Phys. **189**, 261 (1994).
[24] A. I. Krylov, R. B. Gerber, and R. D. Coalson (unpublished).
[25] A. I. Krylov and L. Ya. Baranov (unpublished).